

pH-Dependent Intramolecular Binding and Structure Involving Cx43 Cytoplasmic Domains*

Received for publication, July 12, 2002
Published, JBC Papers in Press, July 31, 2002, DOI 10.1074/jbc.M207016200

Heather S. Duffy^{‡§}, Paul L. Sorgen[¶], Mark E. Girvin[¶], Phyllis O'Donnell^{||}, Wanda Coombs^{**},
Steven M. Taffet^{||}, Mario Delmar^{**} ^{‡‡} §§, and David C. Spray[‡] ^{‡‡}

From the Departments of [‡]Neuroscience and [¶]Biochemistry, Albert Einstein College of Medicine, Bronx, New York 10461, and the Departments of ^{**}Pharmacology and ^{||}Microbiology, Upstate Medical University, Syracuse, New York 13210

pH-induced closure of connexin43 (Cx43) channels involves interaction of the Cx43 carboxyl-terminal (Cx43CT) with a separate “receptor” domain. The receptor location and structure and whether the interaction is directly intramolecular are unknown. Here we show resonant mirror technology, enzyme-linked sorbent assays, and nuclear magnetic resonance (NMR) experiments demonstrating pH-dependent binding of Cx43CT to region 119–144 of Cx43 (Cx43L2), which we propose is the receptor. NMR showed that acidification induced α -helical order in Cx43L2, whereas only a minor modification in Cx43CT structure was detected. These data provide the first demonstration of chemically induced structural order and binding between cytoplasmic connexin domains.

Connexins are integral membrane proteins that oligomerize to form intercellular channels called gap junctions. These channels provide diffusional intercellular exchange of ions and small molecules, allowing individual cell events to synchronize into functional responses of an entire organ. It is the current view that gap junctions are not passive pores but dynamic filters that regulate traffic of molecular messages in time and space through a variety of intermolecular interactions (see, *e.g.* Refs. 1–5).

Intracellular pH is one of the most generic regulators of intercellular communication. Intracellular acidification leads to closure of gap junctions in all native tissues and exogenous expression systems tested (6–8), including channels formed of Cx43, the most abundant gap junction protein in brain and heart. The study of pH-dependent regulation of gap junctions becomes more relevant given that intracellular acidification is a major consequence of tissue ischemia. Acidification-induced uncoupling (also referred to as “pH gating”) has an impact on the preservation of tissue surrounding the ischemic area, both in heart and brain (9, 10) and may be a key substrate for life-threatening arrhythmias during myocardial infarction (9).

Previous studies showed that pH gating of Cx43 results from the interaction of the carboxyl-terminal domain, acting as a

gating particle, with a separate region of the protein affiliated with the pore, acting as the “receptor” (11). These data led to the suggestion that pH regulation of Cx43 follows a “ball-and-chain” model of gating (11, 12). Additional studies showed that the model also applies to Cx43 regulation by insulin, insulin-like growth factor-1, and v-src (13, 14). Yet no conclusive evidence has been presented for a direct intramolecular association between regions of Cx43. Moreover, the location and structure of the receptor for the gating particle remains to be identified.

Here we used mirror resonance (MR),¹ enzyme-linked sorbent assays (ELSA), and nuclear magnetic resonance (NMR) to characterize molecular events associated with chemical regulation of Cx43. We demonstrate pH-dependent binding between two intracellular regions of the molecule: the carboxyl-terminal domain (Cx43CT) and the second half of the cytoplasmic loop (Cx43L2). Furthermore, we show that acidification induces α -helical structure in the Cx43L2 peptide, concurrent with protonation of histidines in the L2 sequence. In contrast, we detected only minor modifications in the structure of Cx43CT as a function of pH. This is the first evidence of organized secondary structure in an intracellular connexin domain consequent to a chemical stimulus and the first demonstration of direct intramolecular binding in a connexin molecule. We hypothesize that this interaction represents part of the structural foundation for the ball-and-chain model of chemical gating. Our data may offer a starting point for the design of molecules that could interfere with the chemical regulation of Cx43 channels.

EXPERIMENTAL PROCEDURES

Production of Purified Recombinant Cx43CT

Cloning of the Cx43CT Fragment—The carboxyl-terminal domain of rat Cx43 (rCx43) was cloned, using the polymerase chain reaction, into the bacterial expression vector pGEX-6P-2 (Amersham Biosciences). This vector contains the coding region of glutathione *S*-transferase (GST) fused to the cleavage site for human rhinovirus 3C protease (see below). The template was produced as previously described (15). To clone the Cx43CT domain, the following primers were used: forward, GAA GGA TCC ATG AGC GAT CCT TAC CAC GCC; and reverse, GCT TGA ATT CCA AGC CGG TTT AAA TCT CC.

Expression of Recombinant GST-Cx43CT—pGEX-6P-2 plasmids containing the GST-Cx43CT insert were transformed into BL-21-competent bacterial cells. Bacteria in LB broth were induced with 0.5 mM isopropyl-1-thio- β -D-galactopyranoside for 3–4 h; bacteria were then

* Supported by National Institutes of Health grants to (to M. D., M. G., and D. C. S.), a Postdoctoral Fellowship (to P. L. S.), and Training Grant NS07098 (to H. D.). The costs of publication of this article were defrayed in part by the payment of page charges. This article must therefore be hereby marked “advertisement” in accordance with 18 U.S.C. Section 1734 solely to indicate this fact.

[‡] Both authors contributed equally to the work.

^{‡‡} Contributed equally by both laboratories.

^{§§} To whom correspondence should be addressed: Dept. of Pharmacology, State University of New York, Upstate Medical University, 766 Irving Ave., Syracuse, NY 13210. Tel.: 315-464-7987; Fax: 315-464-8014; E-mail: delmarm@upstate.edu.

¹ The abbreviations used are: MR, mirror resonance; ELISA, enzyme-linked immunosorbent assay; ELSA, enzyme-linked sorbent assay; GST, glutathione *S*-transferase; Fmoc, *N*-(9-fluorenyl)methoxycarbonyl; PBS, phosphate-buffered saline; Cx43, connexin43; Cx43CT, Cx43 carboxyl-terminal; BSA, bovine serum albumin; TOCSY, total correlation spectroscopy; NOESY, nuclear Overhauser effect spectroscopy; HSQC, heteronuclear single quantum coherence; DQF-COSY, double-quantum-filtered correlation spectroscopy.

washed in phosphate-buffered saline (PBS) at pH 7.4 and pelleted by centrifugation (3000 rpm, 20 min). Bacterial pellets were bathed (20 ml/liter of culture) in PBS containing 1 mM dithiothreitol, 100 μ g of DNase, and 800 μ l of a 25 \times stock of a protease inhibitor mixture ("Complete," Roche Molecular Biochemicals) and sonicated on ice three times for 20 s. The lysate was cleared by centrifugation (20 min, 12,000 rpm; 4 $^{\circ}$ C), and the presence of the fusion protein was confirmed by SDS-PAGE.

Purification of Cx43CT—To purify Cx43CT, bacterial lysate (20 ml) was incubated with 2 ml of glutathione-Sepharose 4B beads (Amersham Biosciences) at 4 $^{\circ}$ C for 2 h while gently rocking. The beads were then washed with PBS, incubated with PBS containing 2 mM ATP and 10 mM MgCl₂ for 20 min at 37 $^{\circ}$ C (to remove a bacterial contaminant), and then washed again (4 \times) with PBS. To cleave the Cx43CT from the GST, the beads were incubated overnight at 4 $^{\circ}$ C with 160 units of PreScission Protease (a commercially available (Amersham Biosciences) fusion protein consisting of GST and the human rhinovirus 3C protease). The recombinant product after cleavage from GST contained the sequence 255–382 of rCx43 preceded by four additional amino acids (GPLG). The eluate was cleared by centrifugation (3000 rpm, 1 h, 4 $^{\circ}$ C) through an Amicon Centriplus 50 (Millipore). The filtrate was collected and then passed through an Amicon Centriplus 10 filter (3000 rpm, 2 h at 4 $^{\circ}$ C). The retentate, containing the purified Cx43CT, was resuspended in a solution of 10 mM Tris, 40 mM KCl, and 1 mM dithiothreitol at pH 7.5.

Protein concentrations were measured using a commercial kit (Bio-Rad DC Protein Assay). Protein purity was assessed by the characteristics of a Coomassie Blue-stained band in a protein gel, and in two separate cases, by mass spectrometry (matrix-assisted laser desorption ionization). In all evaluations, Cx43CT protein was found to be ~90% pure.

Production of ¹⁵N-Labeled Cx43CT—Bacteria were grown as indicated above, but in a minimal medium containing 100 mM KH₂PO₄, 70 mM KOH, 18 mM FeSO₄·7H₂O, 300 mM glucose, 1 mM MgSO₄, 1.48 μ M thiamine, 100 μ g/ml ampicillin, and 0.75 mg/ml ¹⁵NH₄Cl.

Peptide Synthesis

A series of synthetic peptides corresponding to specific sequences of intracellular domains of Cx43 were tested for their association with Cx43CT and, in one case (peptide Cx43L2; see below) to determine secondary structure. Sequences were chosen in part based on predictions of α -helical secondary structure using the structure prediction neural net program, Pred2Ary (16). The names, primary sequences, and amino acid locations in the Cx43 sequence are listed below in Table I. All peptides were synthesized to >95% purity at the Laboratory for Macromolecular Analysis at the Albert Einstein College of Medicine. The syntheses were carried out using Fmoc chemistry on an Applied Biosystems 430A automated peptide synthesizer. Biotinylation of Cx43L2 was accomplished by N-terminal linkage of activated Biotin (Aldrich, St. Louis, MO) using Fmoc- ϵ -aminocaproic acid (Bachem, Torrance, CA). The samples were purified by high-performance liquid chromatography, and purity was assessed by electron ionization mass spectrometry. Peptides were diluted in PBS buffer containing 0.1% Tween 20 (PBST), and the pH was adjusted using small volumes of concentrated HCl or NaOH as appropriate. Purified calmodulin was purchased from a commercial vendor (Sigma) and also tested by MR for its ability to bind to Cx43CT.

Mirror Resonance

Mirror resonance (MR) experiments were performed using an IAsys apparatus as described previously (17–19). Cx43CT was covalently bound to carboxymethyl dextran-coated cuvettes using 1-ethyl-3-(3-dimethylaminopropyl)carbodiimide-HCl (EDC) and N-hydroxysuccinimide (NHS) according to the manufacturer's instructions (Affinity Sensors, Cambridge, England); total cuvette area was 16 mm² and density of matrix-bound Cx43CT was about 5 ng/mm² (calculated from the response obtained during binding, assuming an equivalence of 163 arc-seconds per nanogram per mm² (17)). Ligates (peptides) were added to the cuvettes in PBST and were removed by a 3-min exposure to 10 mM HCl. Control experiments were conducted to determine the binding of the peptide to the matrix itself. For this purpose, a carboxymethyl-dextran cuvette was activated with EDC/NHS in the same manner used to covalently bind Cx43CT (31), except in this case no Cx43CT was included in the mixture. We refer to this as a "blank" cuvette. An average "blank trace" was calculated from three separate experiments in which the change in resonance elicited by a given concentration of a ligate to the blank cuvette was recorded. Blank traces were subtracted from those obtained using a Cx43CT-coated cuvette to determine the binding that was specific to the ligand-ligate interaction.

MR data were acquired and analyzed using the IAsys software package (17). Changes in resonance were recorded for the first 15 min after peptide addition and fit by exponential functions; steady-state responses (arc-seconds) were measured or projected from initial rates. All data measurements ignored the first two points acquired after addition (or washout) of the peptide, because those were considered to be subject to artifactual effects due to changes in the refractive index of the solution (17–19).

Concentration-dependence curves were best-fit by single-exponential functions, as predicted by first-rate order kinetics (17, 18). Consequently, dissociation constants (K_D) were estimated from the concentration of the peptide that elicited a response of one-half the maximal amplitude (17, 18).

Enzyme-linked Sorbent Assay

We developed a colorimetric method, modeled after the "ELISA" technique (enzyme-linked immunosorbent assay), to assess the interaction between Cx43CT and the Cx43L2 peptide. We refer to this method as "ELSA" (enzyme-linked sorbent assay). Briefly, Purified Cx43CT (either 50 or 100 ng/ μ l in PBS at pH 7.4) was added to individual wells of an Immulon-1B plate (100 μ l per well). Bovine serum albumin (1%, pH 7.4) was used as control. The plates were incubated at 2–8 $^{\circ}$ C overnight to allow for adsorption of the ligand (Cx43CT or BSA). Plates were then blocked with 200 μ l of 1% BSA diluted in PBS (pH 7.4) and incubated at 2–8 $^{\circ}$ C overnight. After block, plates were washed with 200 μ l of PBS and 0.05% Tween 20 (PBST) at either pH 6.5 or 7.4 and a PBST solution containing various concentrations of a biotinylated-Cx43L2 synthetic peptide was added to each well (100 μ l per well, pH 6.5 or 7.4). The peptide-containing solution was allowed to interact with the ligand for 2 h. At the end of the incubation time the wells were washed (PBST, pH was held constant) and then 100 ng of horseradish peroxidase-conjugated streptavidin (Pierce Endogen, Rockford, IL) diluted in PBST at pH 6.5 or 7.4 were added for 1 h. After another wash step, 2,2'-azino-bis(3-ethylbenzthiazoline-6-sulfonic acid) substrate (100 μ l, Rockland Immunochemicals, Gilbertsville, PA) was applied and incubated at room temperature for 30 min. Optical density (OD) was measured at A₄₀₅ on a VMAX plate reader (Molecular Devices). The OD value was interpreted as directly indicative of the Cx43L2 concentration non-covalently bound to the ligand.

NMR Spectroscopy

NMR experiments (two-dimensional proton DQF-COSY (20), TOCSY (21), and NOESY (22)) were performed on a Bruker DRX-600 spectrometer at 7 $^{\circ}$ C. Cx43L2 concentrations were ~2 mM for each experiment. NMR data were acquired with 4096 complex t_2 points and 256 t_1 points. Mixing times of 125 and 300 ms were used for the two-dimensional NOESY spectra, and a mixing time of 100 ms was used for TOCSY spectra. Water suppression was achieved by using WATERGATE (23).

Cx43L2 C α and C β chemical shifts were analyzed utilizing natural abundance ¹³C in a ¹H¹³C HSQC (24). HSQC data were acquired with 2048 complex t_2 points and 160 complex t_1 points. Spectral widths of proton and carbon resonances were 8,389 and 12,070 Hz, respectively. The number of scans per t_1 increment was 256.

Hydrogen bonds were identified based on temperature dependence studies (25). The amide proton chemical shifts were followed from 7 $^{\circ}$ C to 37 $^{\circ}$ C. Any amide proton that shifted less than 5.0 ppb/K was considered likely to be hydrogen bonded.

Gradient-enhanced two-dimensional ¹H¹⁵N HSQC experiments (26) were used to observe all backbone amide resonances in ¹⁵N-labeled Cx43CT. Data were acquired with 1024 complex points in the direct dimension and 64 complex points in the indirect dimension. Sweep widths were 8389 Hz in the proton dimension and 2432 Hz in the nitrogen dimension. Amide proton-amide proton NOEs were observed in two-dimensional ¹⁵N NOESY-HSQC spectra (26) collected with 512 and 2048 complex points, for t_1 (H) and t_2 (HN) time domains, and a mixing time of 125 ms.

Translational diffusion coefficients were measured by a bipolar pulse pair longitudinal-eddy-current delay experiment (27). The pK_a values of the histidine side chains were determined from one-dimensional proton spectra collected on a Bruker DRX-300 spectrometer at 27 $^{\circ}$ C. A total of 128 scans was collected into a 16K data block using a sweep width of 6173 Hz for the titration spectra. Lyophilized Cx43L2 peptide was dissolved in 0.6 ml of D₂O PBS buffer for a final concentration of 1 mM. The pH of the solution was adjusted by the addition of either 10 mM NaOD or DCl. The pH values quoted indicate pH measurements of the D₂O solutions uncorrected for the deuterium isotope effect on the glass (28).

TABLE I
Cx43 peptides used and their sequence

Peptide	Cx43 position	Cx43 domain	Amino acid sequence
Cx43NT	1–23	Amino terminus	MGDWSALGKLLDKVQAYSTAGGK
Cx43L1	95–114	First half of cytoplasmic loop	HVFYVMRKEEKLNKKEEELK
Cx43L2	119–144	Second half of cytoplasmic loop	DGVNVEMHLKQIEIKKFKYGIEEHGK
Cx43–271	271–287	Fragment of carboxyl terminus	CSSPTAPLSPMSPPGYK
Cx43–336	336–350	Fragment of carboxyl terminus	DFPDDNQNAKKVAAG
Cx43–346	346–360	Fragment of carboxyl terminus	KVAAGHELQPLAIVD

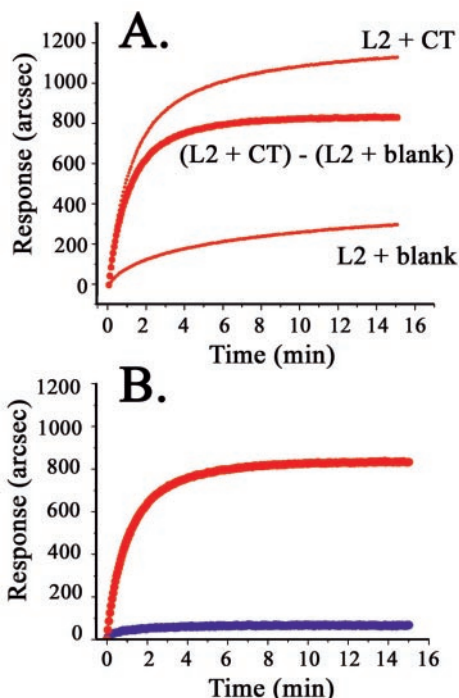


FIG. 1. **Binding determined by mirror resonance of a peptide corresponding to the second half of the cytoplasmic loop (L2) to the carboxyl-terminal (CT) domain of Cx43.** *A*, mirror resonance traces obtained after adding 0.1 mM L2 at pH 6.5 to a cuvette where recombinant Cx43CT had been immobilized (trace labeled “L2+CT”) to a cuvette in the absence of Cx43CT (trace labeled “L2+blank”) and the difference between these responses (trace labeled “(L2+CT)-(L2+blank)”). Note that the subtraction of nonspecific binding removes a slow component comprising about 25% of the total response. At lower peptide concentrations, nonspecific binding was minimal. *B*, pH dependence of Cx43L2-Cx43CT binding. The red trace is the same as the subtracted trace in panel *A* (pH 6.5). The blue trace shows the binding at pH 7.4 of 0.1 mM Cx43L2 to the immobilized Cx43CT.

Proton chemical shifts were referenced directly to internal 3-(trimethylsilyl)propionic acid. Nitrogen referencing was calculated indirectly from the proton referencing (29). All NMR spectra were processed using NMRPip (30), and data were analyzed using NMRView (31).

Model structures were calculated by torsion angle dynamics using the program Dyana (32). NOE cross-peaks classified as strong, medium, and weak were converted into distance restraints of 1.8–2.5, 1.8–3.5, and 1.8–5.5 Å, respectively. Torsion angle restraints were obtained from chemical shift analysis using the TALOS program (33). Hydrogen bonds were imposed as two distance restraints (H-O distance 1.9–2.3 Å and N-O distance of 2.4–3.0 Å). The 10 best minimized structures were evaluated using AQUA and PROCHECK-NMR (34).

RESULTS

Mirror Resonance: Selective Binding of the Cx43L2 Peptide to the Recombinant Cx43CT Protein

We used mirror resonance to test whether Cx43CT binds in a pH-dependent manner to other intracellular regions of Cx43. Recombinant Cx43CT was covalently bound to a carboxymethyl dextran matrix on the surface of a sensor chip, and exposed to various synthetic peptides that correspond to differ-

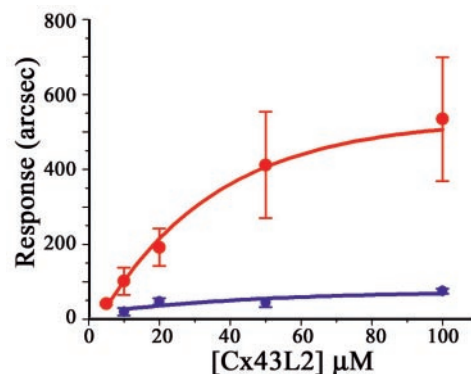


FIG. 2. **Concentration dependence of Cx43L2-Cx43CT binding at pH 7.4 (blue line) and 6.5 (red line) determined by mirror resonance.** The amplitude of the binding at each concentration was determined from the exponential best-fit of the subtracted traces. The data describing the concentration dependence at pH 6.5 was best-fit (least squares) by a monoexponential function. The dissociation constant K_D was estimated from the peptide concentration that corresponded to 50% of maximum binding. The calculated K_D value was 24 μM .

ent intracellular regions of Cx43. Of all peptides tested (see list in Table I), binding was observed only to a peptide corresponding to the second half of the cytoplasmic loop (Cx43L2). A representative trace from experiments applying the highest peptide concentration tested (0.1 mM) is presented in Fig. 1*A* (trace labeled “L2 + CT”). The plot depicts the amplitude of the resonance signal (in arc-seconds) as a function of time. The pH of the solvent for that experiment was 6.5. At such high peptide concentration, but not detectable for concentrations < 50 μM , binding was also detected when peptide Cx43L2 was added to a blank cuvette at the same concentration and pH used in the Cx43CT cuvette, indicating nonspecific binding of Cx43L2 to the matrix. Yet, the amplitude of the binding was much smaller and the rate significantly slower than when the cuvette was coated with Cx43CT. The average blank trace (three separate experiments) for this particular Cx43L2 concentration at pH 6.5 is shown in Fig. 1*A* (trace labeled “L2 + blank”; see “Experimental Procedures” for further details). The nonspecific component of the binding was subtracted from the binding recorded when Cx43L2 was added to the Cx43CT-coated cuvette. As shown by the trace labeled “(L2 + CT) - (L2 + blank)” in Fig. 1*A*, the subtraction eliminated a slow component that was not specific to the interaction of Cx43L2 with Cx43CT.

To examine the pH dependence of the association, the Cx43L2-Cx43CT binding experiment was repeated at pH 7.4. Representative subtracted traces are shown in Fig. 1*B*. Clearly, increasing solvent pH to 7.4 caused a significant reduction in the amplitude of the response. The peptide concentration was 100 μM for both experiments. These data suggest that low pH increases the binding affinity of the Cx43L2 peptide for Cx43CT. It is worth noting that all other peptides tested and the recombinant Ca^{2+} binding protein calmodulin also failed to bind to Cx43CT when the reaction was conducted at a pH of 7.4 (data not shown).

A plot correlating the concentration of Cx43L2 to the ampli-

FIG. 3. Concentration dependence of Cx43L2-Cx43CT binding at pH 7.4 (red lines) and 6.5 (blue lines) determined by an enzyme-linked sorbent assay (ELSA). The concentration of Cx43CT in the solution used to coat the wells was either 50 ng/ μ l (A) or 100 ng/ μ l (B). All data points were best-fit (least squares) by monoexponential functions. Dissociation constant (K_D) values are presented in Table II.

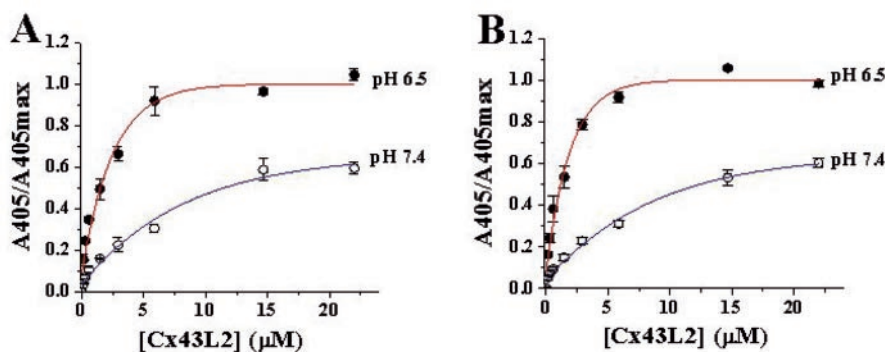


TABLE II
 K_D values of Cx43CT-Cx43L2 binding determined by ELSA

pH	K_D^a	K_D^b
	μ M	
6.5	1.5	1.2
7.4	4.8	5.0

Wells were coated with a solution containing either: ^a 50 ng/ μ l or ^b 100 ng/ μ l of Cx43CT.

tude of the binding is shown in Fig. 2. The data points were calculated from the exponential best-fits of subtracted traces recorded at a pH of 6.5 (red line and symbols) or 7.4 (blue line and symbols). The K_D value of the Cx43CT-Cx43L2 interaction at a pH 6.5, estimated from the concentration-dependence curve of the subtracted traces, was 24 μ M. The amplitude of the binding curve at pH 7.4 was too small to be properly fit; therefore, K_D values for the binding at pH 7.4 could not be calculated under these conditions. Altogether, the results demonstrate selective, pH-dependent, and concentration-dependent binding between the carboxyl-terminal domain and the second half of the cytoplasmic loop of Cx43.

Cx43L2-Cx43CT Binding Determined by the ELSA Method

Binding of Cx43CT to Cx43L2 was also demonstrated using an ELISA-like binding assay (see “Experimental Procedures”). Concentration-dependence curves are shown in Fig. 3. Panels A and B correspond to data obtained from plates coated with Cx43CT at a concentration of 50 and 100 ng/ μ l, respectively. In both plots, the abscissas indicate the concentration of Cx43L2 added to the plate, and the ordinates correspond to the extent of binding. The data points depict the averages of three separate experiments, each in duplicate. Bars indicate the standard error of the mean. Closed circles represent data obtained when the binding assay was performed at pH 6.5, and open circles correspond to values obtained at pH 7.4. Consistent with our results using mirror resonance, the amplitude of the binding increased when the pH of the solvent was reduced. To facilitate comparisons, all experimental values were normalized to the magnitude of the asymptote describing the binding of Cx43L2 to Cx43CT at pH 6.5. Data points were best-fit by single-exponential functions. The monoexponential increase in the amplitude of the binding as a function of ligate concentration suggested that this interaction could be described by first-rate order kinetics (36). Accordingly, we determined the dissociation constant (K_D) from the concentration of the ligate that corresponded to 50% of maximum binding. Values are presented in Table II. No sizable difference was detected as a function of the concentration of Cx43CT used to coat the plates, further confirming the applicability of first-rate order kinetics. The K_D value was decreased 3- to 4-fold when the experiment was performed at low pH. No significant binding was detected when BSA (75 ng/ μ l) was used as ligate, neither was binding ob-

TABLE III
Translation diffusion coefficient

Cx43L2		Cx43CT		Cx43L2/Cx43CT	
pH 5.8	pH 8.0	pH 5.8	pH 8.0	pH 5.8	pH 8.0
$D_s \times 10^{-6} \text{ cm}^2/\text{s}$					
A 1.45	1.24	D 0.37	0.40	A 0.59	1.62
B 1.37	1.40			B 0.56	1.45
C 1.48	1.35			C 0.51	1.52

served when Cx43L2 was added to plates not coated, or coated with BSA (data not shown). These results confirm the pH dependence of Cx43CT-Cx43L2 binding obtained by MR and indicate that acidification of the solvent increases the binding affinity of Cx43L2 for the CT domain.

Nuclear Magnetic Resonance

Translational Diffusion Analysis—pH-dependent binding of Cx43L2 to Cx43CT was independently confirmed by translational diffusion analysis using NMR. This technique characterizes the diffusion coefficient (D_s) of a given molecule within a pulsed magnetic field gradient, based on the size of the molecular complex (27). Spectra were obtained from samples containing either Cx43L2 (1.0 mM), Cx43CT (1.0 mM), or both (0.5 mM of Cx43L2 and 0.5 mM of Cx43CT). The samples were in PBS and buffered at a pH of either 8.0 or 5.8. These pH values were chosen, because they fall within the asymptotes of the titration curve of Cx43L2 (see below). Three specific non-overlapping resonances of Cx43L2 were followed both in the absence and in the presence of Cx43CT. Data from those resonances are labeled A, B, and C in Table III. The diffusion coefficient obtained from a Cx43CT resonance (labeled D) is shown for comparison. The low diffusion rate measured experimentally for Cx43CT suggests that this molecule either adopts an extended conformation or oligomerizes. No pH-dependent differences in mobility were detected for either Cx43CT or Cx43L2 alone. The Cx43L2 diffusion coefficient decreased in the presence of Cx43CT at low pH. However, at pH 8.0, the Cx43L2 diffusion coefficient in the presence of Cx43CT was similar to that of Cx43L2 alone. These results indicate that Cx43L2 binds, in a pH-dependent manner, to Cx43CT, and are consistent with those obtained using both ELSA and MR. In the context of the particle-receptor hypothesis for pH gating (11), these results lead to the suggestion that the second half of the cytoplasmic loop contains at least part of the receptor for the Cx43CT gating particle.

pH-dependent Cx43CT Structure—Intermolecular binding often requires a structural rearrangement of the molecules involved. We therefore performed NMR experiments to test whether acidification caused a change in the secondary structures of either fragment. Gradient-enhanced two-dimensional $^1\text{H}^{15}\text{N}$ HSQC experiments (26) were used to observe all backbone amide resonances in ^{15}N -labeled Cx43CT dissolved in

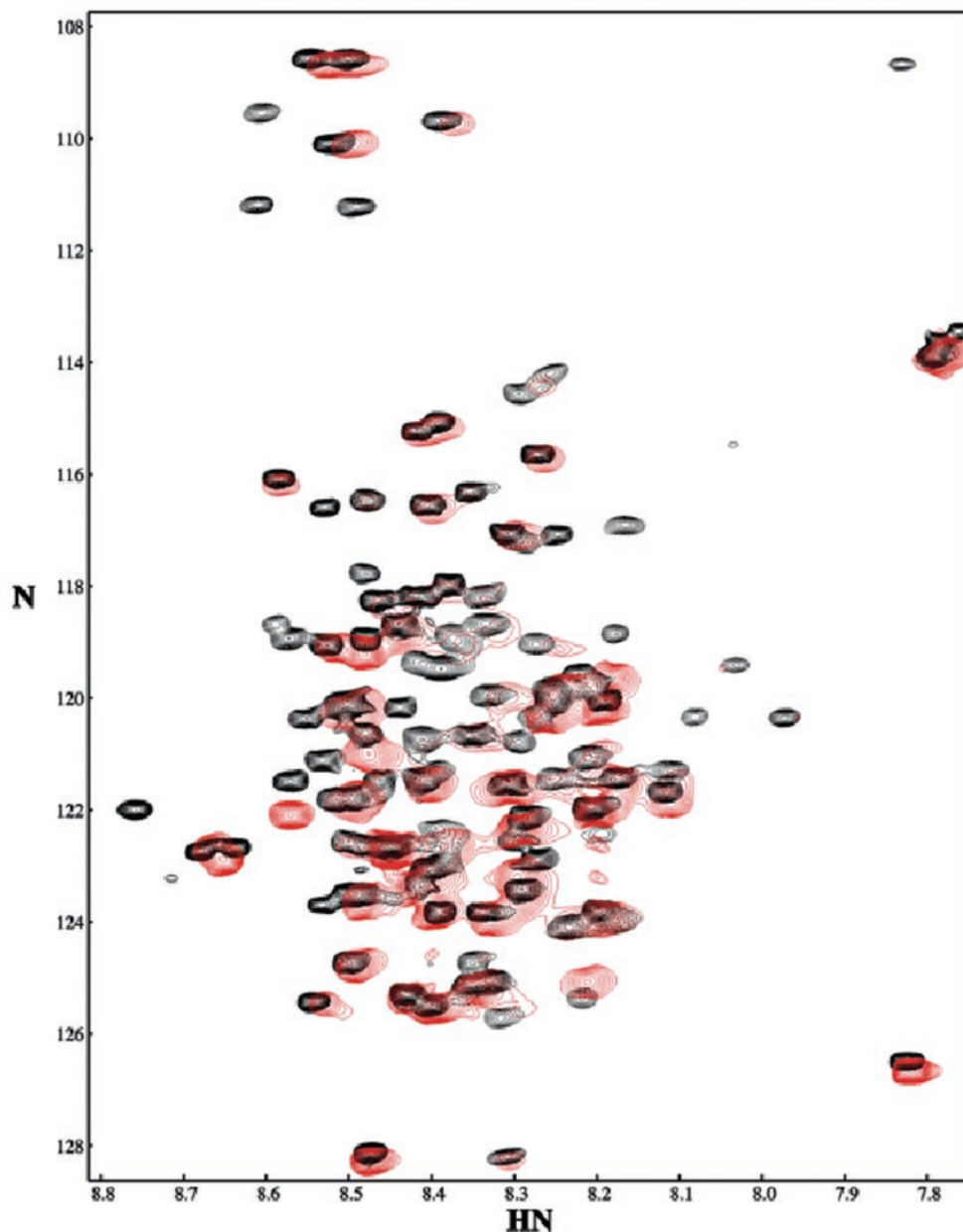


FIG. 4. $^1\text{H}^{15}\text{N}$ HSQC of the carboxyl-terminal domain of rat Connexin43 (Cx43CT). The spectra were recorded using 1.0 mM Cx43CT in PBS buffer at 7 °C buffered to pH 8.0 (red) or 5.8 (black).

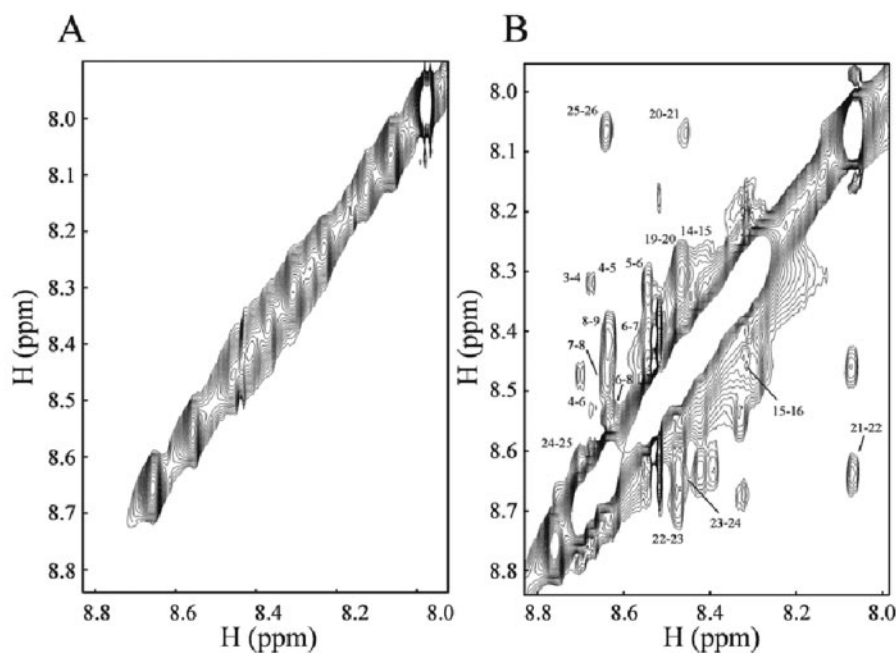
PBS at various pH values. Fig. 4 shows the cross-peaks obtained at pH 8.0 (red) and at pH 5.8 (black). The wide dispersion of cross-peaks in the spectra indicates that at both pH values there was a degree of structural order within the molecule. However, acidification caused only a minor shift in a number of peaks, suggesting that the structure of the Cx43CT was not substantially modified by the pH of the solvent within the range tested.

pH-dependent Conformational Change of Cx43L2—Acidification had a dramatic effect on the structural organization of the Cx43L2 peptide, as shown by the ^1H NOESY spectra presented in Fig. 5. Nuclear Overhauser effect spectroscopy (NOESY) identifies specific through-space polarization transfers and therefore offers a view of the type and extent of structural order present in the protein. The absence of through-space transfers is indicative of lack of organized structure and correlates with

a NOESY spectrum that does not depart away from the diagonal line. Clearly, a drop in the pH from 8.0 (panel A) to 5.8 (panel B) induced a large increase in the number of inter-residue cross-peaks (*i.e.* contours that can be detected off of the diagonal). Numbers 1–26 in panel B identify the signals from amino acids 119 to 144 of Cx43. These data indicated through-space interactions consistent with the formation of secondary (α -helical) structure in response to acidification. We therefore pursued a detailed structural analysis of Cx43L2 at low pH.

Titration of Histidine Side Chains—pH-dependent changes in the structure and/or function of a protein result from protonation of amino acid side chains. The range of pH values associated with increased Cx43CT-Cx43L2 binding (Fig. 1), as well as the range of pH values corresponding to Cx43 pH gating (11, 35) was near the pK_a value for histidine residues (36). We therefore tested whether the effect of acidification on Cx43CT-

FIG. 5. Amide proton region from a two-dimensional ^1H - ^1H NOESY of the Cx43L2 peptide at 7 °C for pH values 8.0 (A) and 5.8 (B). The Cx43L2 peptide numbers 1–26 correspond to the Cx43 sequence numbers 119–144.



Cx43L2 binding could be associated with the protonation of histidines in Cx43L2. Fig. 6A shows the ^1H NMR spectra of Cx43L2 dissolved in D_2O at various pH values. Protonation or deprotonation changes the charge of a side chain and, consequently, the electron density surrounding the nuclei. As a result, a change in the chemical shift would be observed. Thus, a pH-induced shift in the position of a peak is reflective of a change in the protonation state of the amino acid associated with that particular peak. Acidification of the solvent led to a progressive change in chemical shift of two particular peaks in the spectra, corresponding to the C-2 ring protons from His¹²⁶ and His¹⁴². A plot of chemical shift as a function of pH is presented in panel B. The observed pK_a values were 6.83 for His¹²⁶ and 6.79 for His¹⁴². The data demonstrate that acidification of the solvent leads to protonation of two specific side chains of the peptide. The result supports the notion that histidine protonation is a step in the conformational change associated with low pH and in the acidification-induced closure of the gap junction channel (37–39).

Cx43L2 Amino Acid Assignments and Secondary Structure—Amino acid spin systems and their sequential assignments were identified by DQF-COSY, TOCSY, and NOESY spectra. As noted above, NOE interactions reflect transfers of magnetization through space. Furthermore, quantitative information on the distances between backbone protons can be derived from the intensities of the cross-peaks. From those distances, inferences on spatial constraints can be made. A summary of the various backbone NOE interactions obtained from Cx43L2 at pH 5.8 is depicted in Fig. 7. To facilitate the presentation of the data, cross-peak intensities are represented by the *thickness* of the *horizontal line*. We identified transfers between amide protons (NN), between protons associated with the alpha or beta carbons and the amide protons (αN , βN) and transfers between alpha and beta carbon protons ($\alpha\beta$). These transfers were detected between a given amino acid (i) and another residue downstream (1 . . . 4). Unresolved assignments due to spectral overlap are depicted by *gray bars*. The data show a break in backbone connectivities between amino acids Lys¹²⁸ and Gly¹³⁸. Outside that intermediate area, the overall pattern was consistent with a modestly stable helical structure. The predominant regions of helical structure are noted by the *black*

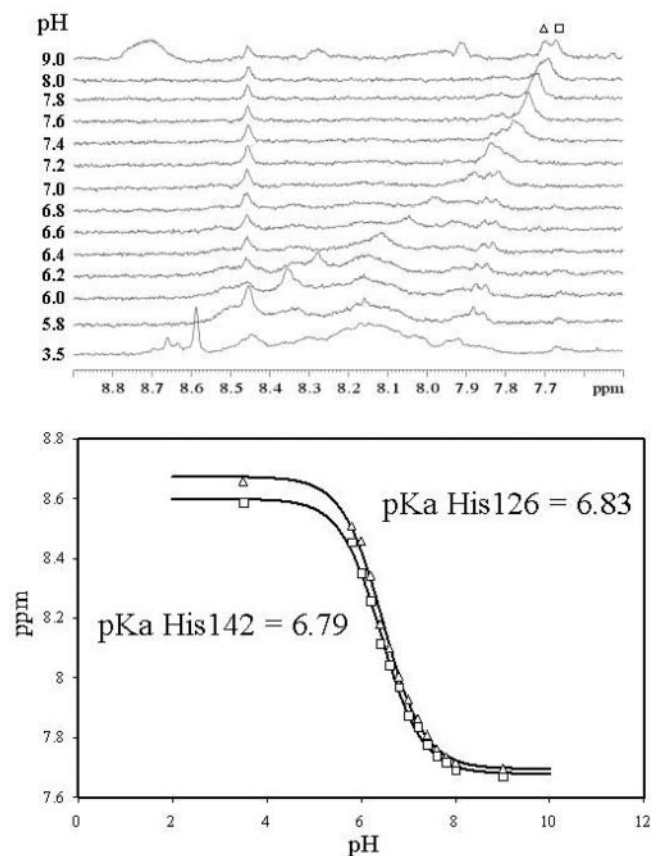


FIG. 6. pH titration of Cx43L2 histidine side chains as detected by 300 MHz ^1H NMR (8.9–7.5 ppm) at 25 °C. The ^1H NMR spectra at various pHs (top) and the corresponding pH titration curve (below) were fitted to the equation, $\delta = \delta_{\text{min}} + (\delta_{\text{max}} - \delta_{\text{min}})/(1 + 10^{\text{pH}-\text{pK}_a})$, where δ = chemical shift. The *triangles* and *squares* represent the chemical shifts of the His¹²⁶ and His¹⁴² C-2 ring protons.

bars above the Cx43L2 sequence. These regions are in the amino and carboxyl ends of the sequence, where hydrogen bonds (noted by *solid circles*) were observed.

Three-dimensional Structure of Cx43L2 at Low pH—Struc-



FIG. 7. Summary of NMR restraints derived for the Cx43L2 peptide. The filled circles indicate hydrogen bonding determined from variable temperature experiments. The horizontal lines identify backbone NOEs with thicknesses indicating approximate cross-peak intensity. The black bars above the Cx43L2 sequence indicate the regions of helical structure. The gray bars represent unresolved assignments due to spectral overlap.

ture calculations by torsion angle dynamics led to the family of structures shown in Fig. 8 (A and B). The structures were superimposed using the backbone coordinates from Asn¹²²-Gln¹²⁹ and Lys¹³⁶-Gly¹⁴³, not including a poorly defined backbone region (Xaa¹³⁰-Xaa¹³⁵) in the central section. Altogether, 85 restraints were intra-residue, 62 were short range, and 14 were medium range. The total root mean square deviations for these alignments were 0.2 and 0.3 Å, respectively. The structural models fit the NMR data well, with no violations of experimental distance restraints greater than 0.4 Å. A schematic representation of the structure, including the position of the imidazole rings in His¹²⁶ and His¹⁴², is shown in Fig. 8C. Interestingly, the two regions with stronger helical characteristics contain the histidines that may present the binding site for the interaction of Cx43L2 to Cx43CT.

DISCUSSION

The results in this report represent the first demonstration of direct intramolecular binding between cytoplasmic domains of a connexin molecule, and the first evidence of structural modifications of a connexin domain in response to a chemical regulator of junctional communication. The data support and greatly expand the ball-and-chain model for chemical gating of Cx43 (11, 40) and emphasize the potential importance of histidine protonation in pH gating (37, 39). These results open the door for further structural analysis of the Cx43CT and Cx43L2 fragments. Before discussing the implications of our findings, some technical limitations need to be considered.

Technical Limitations—All of the studies reported here were conducted with synthetic peptides and recombinant proteins diluted in a saline buffer at either room or low temperature. The conditions of the reaction are therefore far from those present when a connexin molecule oligomerizes into a functional gap junction in a mammalian cell. Indeed, the folding of the different protein domains and their ability to bind may be affected by environmental conditions such as ionic strength, temperature, and proximity to the membrane lipids. Moreover, protein folding and binding could be limited by steric constraints imposed by the covalent association of the binding elements with the rest of the connexin sequence. The non-covalent associations of the CT domain with other partner molecules (e.g. ZO-1 (1), v-src (2, 14), β-catenin (4), caveolin (41), p120-catenin (5)) could also affect intramolecular binding. Finally, the possibility of accessory proteins involved in Cx43 folding, although never documented, cannot be discarded. Thus, as in any molecular study conducted *in vitro* (including structural determinations (42)), direct extrapolation between

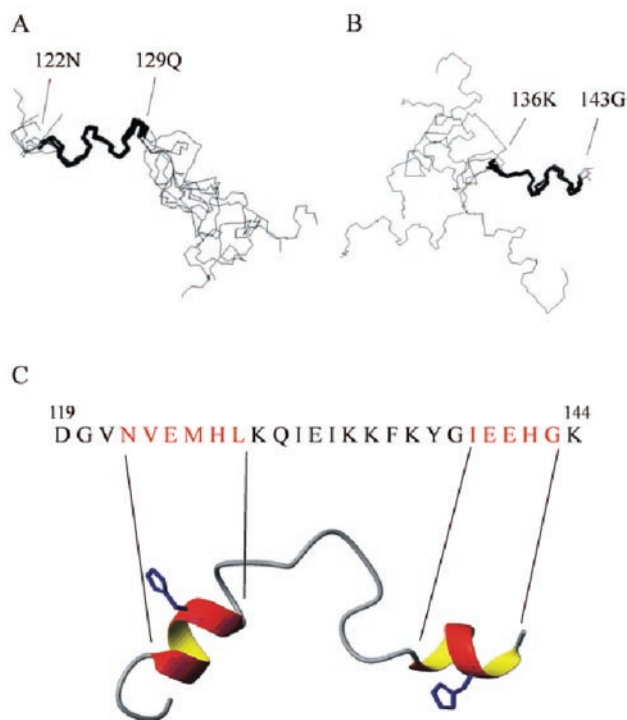


FIG. 8. Solution structure of the Cx43L2 peptide in PBS buffer pH 5.8 at 7 °C. Backbone traces of the 10 Cx43L2 peptide conformers that best represent the structure are aligned by superimposing the backbone atoms (bold) of residues 122N-129Q (A) and 136K-143G (B). Panel C illustrates the helical regions (red/yellow) for the lowest energy Cx43L2 structure. The Cx43L2 sequence is labeled, and the amino acids comprising the α-helix are red. The histidine side chains are blue. All images were produced using MOLMOL (55).

the data presented in this report and the mechanisms of chemical gating of Cx43 needs to be done with caution. However, it is worth noting that: (a) There are a number of examples in the literature showing that two molecular domains that bind in living cells also bind as separate fragments *in vitro* (43, 44). (b) A recombinant Cx43CT protein maintains its ability to react *in vitro* with molecular partners that are biologically active in intact cells (45, 46). (c) Studies in *Xenopus* oocytes, as well as in mammalian cells, show that a free Cx43CT domain interacts with a separate region of the connexin molecule (11, 47, 48) and, in oocytes at least, it does so in a pH-dependent manner. These similarities of function between two systems are consistent with the possibility that the Cx43CT-Cx43L2 interaction observed *in vitro* also occurs in endogenous channels and mediates the pH gating process. Further experiments will assess whether strategies designed to interfere with CT-L2 binding would also prevent pH gating of gap junctions in living cells.

Some differences in the quantitative aspects of our results also deserve consideration. In particular, the amplitude of the binding at pH 7.4 was almost negligible in the case of the MR experiment, although clearly detectable by ELSA. In addition, the K_D values recorded by ELSA for pH 6.5 were 10–20 times lower than those determined by MR. The reasons for these discrepancies are unclear, but one important difference between the two methods is in the way in which the Cx43CT is immobilized in the assays. For MR, free amides are covalently linked to the matrix; for ELSA, the ligand is adsorbed to the bottom of the well. It is likely that the conformation of the protein and its ability to bind be affected differently by its attachment to the dish. Regardless of these quantitative differences, the results demonstrate pH-dependent binding of the L2 peptide to the Cx43CT fragment, with dissociation constants in the micromolar range.

Applicability of These Results to Other Connexin Isoforms—Acidification-induced closure is a phenomenon common to all gap junctions (including those in invertebrates); yet, significant differences exist in the pH sensitivities and domain dependence among the connexin family (8). Although the data presented in this report should be interpreted as relevant only to Cx43 and not necessarily to other connexin isoforms, it is worth noting that results from Peracchia's laboratory indicate that intramolecular as well as intermolecular interactions may be involved in the regulation of Cx32 by pH (50). Further studies will be necessary to address the structural characteristics that make pH gating a phenomenon common to all connexin isoforms. Our working hypothesis is that the functional domains involved in pH regulation may be common to all connexins but may share little homology in terms of primary sequence and topological position within the sequence.

A Direct Role for Protons on pH Gating—One of the issues that has been controversial through the years is whether pH gating is a direct result of proton-protein interaction (37, 49), or whether intermediary molecules are involved (50). The results in this paper demonstrate a direct Cx43CT-Cx43L2 interaction that is pH-dependent. In the particle-receptor model analogy, this would suggest that the affinity of the particle for the receptor increases solely as a consequence of increased proton concentration, which may be important in short-term gating of the channel. Yet, it is now clear that connexins do not stand alone in the membrane but rather exist as central structures in molecular complexes (or "nexus" (51)). Moreover, preliminary evidence from our laboratories suggests that intracellular acidification leads to binding of the SH3 domain of src to Cx43, and consequent dissociation of Cx43 from ZO-1 (52). Other interactions may also take place. Studies of Peracchia *et al.* (50) have suggested that calmodulin may be involved in the regulation of connexins by pH. We failed to detect a Cx43CT-calmodulin interaction, but this may be due to limitations of the MR method, the regions of Cx43 included in our construct, or the possibility that the interaction with calmodulin may be indirect. Overall, the entire pH-gating process may be complex, consisting of both intra- and intermolecular interactions, and the present results likely describe only one piece of the puzzle.

pH-dependent Change in Cx43L2 Conformation: Role for Histidine Residues?—NMR data show that acidification led to a concomitant conformational change in the Cx43L2 peptide and protonation of the histidine residues. Histidine protonation may facilitate the stabilization of a secondary structure, perhaps by interacting with negatively charged amino acid chains in its vicinity. The results suggest that the Cx43L2 fragment may act as a pH sensor to trigger channel closure (38). This hypothesis will be addressed by future experiments testing the pH sensitivity of Cx43 mutants where either one or both of the histidines in the corresponding Cx43L2 sequence are modified. Also, previous studies had indicated that a histidine not part of Cx43L2 (His⁹⁵) might be involved in pH gating (39). Protonation of His⁹⁵ may be part of the conformational change in the loop structure that facilitates Cx43CT-Cx43L2 binding.

L2-CT Association and the "Ball-and-Chain" Hypothesis—Our results represent the first demonstration of direct intramolecular binding between cytoplasmic connexin domains. In the context of the ball-and-chain hypothesis, we propose that the L2 fragment is part of the receptor for the CT domain, which acts as a gating particle. Moreover, we suggest that acidification of the intracellular space is sensed by the histidines in the Cx43L2 sequence. Protonation of these residues would lead to the formation of α -helices. The pH-induced modifications in secondary structure would increase the CT-L2 binding affinity

with at least two fundamental consequences: to precipitate channel closure and to modify the ability of the CT domain to interact with other molecular partners. Under this scenario, pH gating would also involve changes in the composition of the molecular nexus. The nature of the intermolecular interactions and their relevance to the actual process of acidification-induced closure remain to be determined.

Toward a Structural Understanding of Cx43 Regulation—With the exception of a recent report on the structure of the amino-terminal of Cx26 (53), structural information on the cytoplasmic domains of connexins is totally lacking. (Although Unger *et al.* (42) recently described the structure of the pre-forming region of Cx43, they achieved a clear view of the channel through deletion of the carboxyl-terminal domain from the Cx43 construct.) The results presented here are thus the first demonstration of structural order in the carboxyl-terminal and the cytoplasmic loop domains of a connexin molecule. The crucial variable in our case for the study of the Cx43L2 fragment has been the use of low pH. The structural study of Cx43L2 reveals the presence of two short α -helices, stabilized by hydrogen bonds. We speculate that those helices present the interface for the binding of Cx43L2 to Cx43CT. Coil-coil interactions between protein domains that are distant in primary sequence have been shown for numerous proteins (54). Our results lead to the exciting possibility of using NMR to resolve the separate three-dimensional structure of the L2 fragment in its CT-bound configuration. Additional studies will be directed at identifying and localizing structural order in the CT domain alone as well as bound to Cx43L2. These efforts will provide essential information for an intimate understanding of the molecular dynamics of connexin regulation.

Acknowledgments—We gratefully acknowledge the assistance of Dr. Ruth Angeletti and Edward Nieves of the Laboratory of Molecular Analysis and Proteomics (Albert Einstein College of Medicine) for peptide synthesis and mass spectroscopy of peptides and recombinant Cx43CT.

REFERENCES

- Giepmans, B. N., and Moolenaar, W. H. (1998) *Curr. Biol.* **8**, 931–934
- Toyofuku, T., Akamatsu, Y., Zhang, H., Kuzuya, T., Tada, M., and Hori, M. (2000) *J. Biol. Chem.* **276**, 1780–1788
- Lampe, P. D., and Lau, A. F. (2000) *Arch. Biochem. Biophys.* **384**, 205–215
- Ai, Z., Fischer, A., Spray, D. C., Brown, A. M. C., and Fishman, G. I. (2001) *J. Clin. Invest.* **105**, 161–171
- Xu, X., Li, W. E., Huang, G. Y., Meyer, R., Chem, T., Luo, Y., Thomas, M. P., Radice, G. L., and Lo, C. W. (2001) *J. Cell Biol.* **154**, 217–230
- Spray, D. C., and Bennett, M. L. V. (1985) *Annu. Rev. Physiol.* **47**, 281–303
- Francis, D., Stergiopoulos, K., Ek-Vitorin, J. F., Cao, F.-L., Taffet, S. M., and Delmar, M. (1999) *Dev. Genet.* **24**, 123–136
- Stergiopoulos, K., Alvarado, J. L., Mastroianni, M., Ek-Vitorin, J. F., Taffet, S. M., and Delmar, M. (1999) *Circ. Res.* **84**, 1144–1155
- Peters, N. S., Coromilas, J., Severs, N. J., and Wit, A. L. (1997) *Circulation* **95**, 988–996
- Lin, J. H., Weigel, H., Cotrina, M. L., Liu, S., Bueno, E., Hansen, A. J., Hansen, T. W., Goldman, S., and Nedergaard, M. (1998) *Nat. Neurosci.* **1**, 494–500
- Morley, G. E., Taffet, S. M., and Delmar, M. (1996) *Biophys. J.* **70**, 1294–1302
- Zagotta, W. N., Hoshi, T., and Aldrich, R. W. (1990) *Science* **250**, 568–571
- Homma, N., Alvarado, J. L., Coombs, W., Stergiopoulos, K., Taffet, S. M., Lau, A. F., and Delmar, M. (1998) *Circ. Res.* **13**, 27–32
- Zhou, L., Kasperek, E. M., and Nicholson, B. J. (1999) *J. Cell Biol.* **144**, 1033–1045
- Yahuaca, P., Ek-Vitorin, J. F., Rush, P., Delmar, M., and Taffet, S. M. (2000) *Braz. J. Med. Biol. Res.* **33**, 399–406
- Chandonia, J.-M., and Karplus, M. (1999) *Proteins: Struct. Funct. Genet.* **35**, 293–306
- George, A. J., French, R. R., and Glennie, M. J. (1995) *J. Immunol. Methods* **183**, 51–63
- Salamon, Z., Brown, M. F., and Tollin, G. (1999) *Trends Biochem. Sci.* **24**, 213–219
- Duffy, H. S., Delmar, M., Coombs, W., Taffet, S. M., Hertzberg, E. L., and Spray, D. C. (2001) *Cell Adhes. Commun.* **8**, 225–229
- Rance, M., Sorensen, O. W., Bodenhausen, G., Wagner, G., Ernst, R. R., and Wuthrich, K. (1983) *Biochem. Biophys. Res. Commun.* **117**, 479–485
- Davis, D. G., and Bax, A. (1985) *J. Am. Chem. Soc.* **107**, 2820–2821
- Macura, S., and Ernst, R. R. (1980) *Mol. Phys.* **41**, 95–117
- Piotto, M., Saudek, V., and Sklenar, V. (1992) *J. Biomol. NMR* **2**, 661–665
- Bax, A., Clore, G. M., Driscoll, P. C., Gronenborn, A. M., Ikura, M., and Kay, L. E. (1990) *J. Magn. Reson.* **87**, 620–627

25. Baxter, N. J., and Williamson, M. P. (1997) *J. Biomol. NMR* **9**, 359–369
26. Kay, L. E., Keifer, P., and Saareinen, T. (1992) *J. Am. Chem. Soc.* **114**, 10663–10665
27. Wu, D., Chen, A., and Johnson, C. S., Jr. (1995) *J. Magn. Reson. A* **115**, 260–264
28. Glasoe, P. K., and Long, F. A. (1960) *J. Phys. Chem.* **64**, 188–190
29. Wishart, D. S., Bigam, C. G., Yao, J., Abildgaard, F., Dyson, H. J., Oldfield, E., Markley, J. L., and Sykes, B. D. (1995) *J. Biomol. NMR* **6**, 135–140
30. Delaglio, F., Grzesiek, S., Vuister, G. W., Zhu, G., Pfeifer, J., and Bax, A. (1995) *J. Biomol. NMR* **6**, 689–707
31. Johnson, B. A., and Blevins, R. A. (1994) **4**, 603–614
32. Guntert, P., Mumenthaler, C., and Wuthrich, K. (1997) *J. Mol. Biol.* **273**, 283–298
33. Cornilescu, G., Delaglio, F., and Bax, A. (1999) *J. Biomol. NMR* **13**, 289–302
34. Lastowsky, R. A., Rullmann, J. A., MacArthur, M. W., Kaptein, R., and Thornton, J. M. (1996) *J. Biomol. NMR* **8**, 477–486
35. Calero, G., Kanemitsu, M., Taffet, S. M., Lau, A., and Delmar, M. (1998) *Circ. Res.* **82**, 929–935
36. Creighton, T. E. (1993) *Proteins: Structures and Molecular Properties*, pp. 338–340, W. H. Freeman and Company, New York, NY
37. Spray, D. C., Harris, A. L., and Bennett, M. V. L. (1981) *Science* **211**, 712–715
38. Spray, D. C., and Burt, J. M. (1990) **258**, C195–C205
39. Ek, J. F., Delmar, M., Perzova, R., and Taffet, S. M. (1994) *Circ. Res.* **74**, 1058–1064
40. Delmar, M. (2000) *J. Cardiovasc. Electrophysiol.* **11**, 118–120
41. Schubert, A. L., Schubert, W., Spray, D. C., and Lisanti, M. P. (2002) *Biochemistry* **41**, 5754–5764
42. Unger, V. M., Kumar, N. M., Gilula, N. B., and Yeager, M. (1999) *Science* **283**, 1176–1180
43. Sheng, M., and Sala, C. (2001) *Annu. Rev. Neurosci.* **24**, 1–29
44. Mayer, B. J. (2001) *J. Cell Sci.* **114**, 1253–1263
45. Warn-Cramer, B. J., Lampe, P. D., Kurata, W. E., Kanemitsu, M. Y., Loo, L. W., Eckhart, W., and Lau, A. F. (1996) *J. Biol. Chem.* **271**, 3779–3786
46. Lin, R., Warn-Cramer, B. J., Kurata, W. E., and Lau, A. F. (2001) *J. Cell Biol.* **154**, 815–828
47. Anumonwo, J. M. B., Taffet, S. M., Gu, H., Chanson, M., Moreno, A. P., and Delmar, M. (2001) *Circ. Res.* **88**, 666–673
48. Moreno, A., Chanson, M., Anumonwo, J. M. B., Scerri, I., Gu, H., and Delmar, M. (2002) *Circ. Res.* **90**, 450–457
49. Trexler, E. B., Bukauskas, F. F., Bennett, M. V., Bargiello, T. A., and Verselis, V. K. (1999) *J. Gen. Physiol.* **113**, 721–742
50. Peracchia, C., Sotki, S. A., Wang, X. G., Peracchia, L. L., and Persechini, A. (2000) *J. Biol. Chem.* **275**, 26220–26224
51. Spray, D. C., Duffy, H. S., and Scemes, E. (2000) *Adv. Exp. Med. Biol.* **468**, 339–357
52. Duffy, H. S., Sorgen, P., Urban, M., Ashton, A., Coombs, W., Taffet, S. M., Kojima, T., Girvin, M., Delmar, M., and Spray, D. C. (2001) *Soc. Neurosci. Abstr.* **27**, 330.19 (online)
53. Purnick, P. E., Benjamin, D. C., Verselis, V. K., Bargiello, T. A., and Dowd, T. L. (2000) *Arch. Biochem. Biophys.* **381**, 181–190
54. Nusrat, A., Chen, J. A., Foley, C. S., Liang, T. W., Tom, J., Cromwell, M., Quan, C., and Mrsny, R. J. (2000) *J. Biol. Chem.* **275**, 29816–29822
55. Koradi, R., Billeter, M., and Wuthrich, K. (1996) *J. Mol. Graph.* **14**, 51–55